Fortschr. Phys. **61**, No. 2 – 3, 291 – 304 (2013) / **DOI** 10.1002/prop.201200065

Open quantum dots: Physics of the non-Hermitian Hamiltonian

D. K. Ferry[1,*], **R. Akis**[1], **A. M. Burke**[1,5], **I. Knezevic**[2], **R. Brunner**[3], **R. Meisels**[3], **F. Kuchar**[3], and **J. P. Bird**[4]

[1] School of Electrical, Computer, and Energy Engineering, Arizona State University, Tempe AZ 85287-5706, USA
[2] Department of Electrical Engineering, University of Wisconsin, Madison WI 53706, USA
[3] Institut für Physik, Montanuniversität Leoben, 8700 Leoben, Austria
[4] Department of Electrical Engineering, University at Buffalo, Buffalo, NY 14260, USA
[5] School of Physics, The University of New South Wales, Sydney, Australia

Received 31 March 2012, revised 31 March 2012, accepted 16 April 2012
Published online 9 May 2012

Key words Semiconductor quantum dots, classical to quantum transition, projection algebra, dissipation.

Quantum dots provide a natural system in which to study both classical and quantum features of transport, as they possess a very rich set of eigenstates.When coupled to the environment through a pair of quantum point contacts, these dots possess a mixed phase space which yields families of closed, regular orbits as well as an expansive sea of chaos. In this latter case, many of the eigenstates are decohered through interaction with the environment, but many survive and are referred to as the set of pointer states. These latter states are described by a projected, non-Hermitian Hamiltonian which describes their dissipation through many-body interactions with particles in the external environment.

1 Introduction

Since the beginning of quantum mechanics, the measurement of open quantum systems has been of great interest. The earliest papers addressed directly results of measurements. Indeed, measurements have always been considered to be classical, as the results appear in the laboratory. But, to make the measurement, the quantum system must be opened so that it can communicate with the external environment in which the measurement is made. While this is an exceedingly broad topic, measurements on open quantum dots have shown to be an interesting window onto the general measurement problem for quantum systems and how the quantum nature evolves into the classical nature [1]. The subject of quantum dots itself is a quite broad topic [2]. Our interest is in quantum dots formed by electrostatic gates on the surface of a heterostructure, such as GaAs/AlGaAs, in which a two-dimensional electron gas resides at the interface [3], or in similar dots defined by in-plane gates.

Early measurements of such open quantum dots clearly exhibited conductance fluctuations, presumably due to interference effects within these dots [4–9]. These experiments were often interpreted in terms of an earlier theory which suggested that these fluctuations were due to chaotic behavior, with the quantum transport being determined from knowledge of the irregular classical scattering dynamics of the same structures [10, 11]. In such a picture, the quantum mechanics would be completely washed out in the open quantum dot. Later studies, however, showed that the quantum properties were not washed out, but remained robust within the dot, and that scarred wave functions appeared with regular periodic energy

* Corresponding author E-mail: ferry@asu.edu

eigenstates [12], and that this behavior would persist irrespective of whether the structure were classically regular or chaotic [13].

So, quantum states persist in the open quantum dots and wave function scars are stable, both of which could be observed in the oscillatory magneto-conductance of these dots. Which brings us back to the measurement problem. In these dots, as well as in quantum information and computation, the border where the two worlds of classical and quantum mechanics meet is of great relevance due to the problem of measurement. To this discussion, Zurek brought the decoherence theory [14], in which he used the *ansatz* that, in an open system, the environment imposes so-called superselection rules by preserving part of the information that resides in the classical correlations between the system and the measuring apparatus, leading to an environment-induced process of superselection (einselection) [14]. This means that essentially preferred states (which are termed pointer states) survive the decoherence process related to the coupling with the environment. The promotion of certain information, which couples throughout the spectrum of states, in a quantum system due to a natural selection process is known as Quantum Darwinism [15, 16]. Quantum Darwinism is based on the Darwinian concept [17] for the rules of reproduction, heredity, and variation. The pointer states are not only characterized by their robustness, despite the existing environment, but also by their ability to create "offspring" of the states which means they advertise the information about themselves throughout the spectrum. This ability makes it possible for different observers to measure the same information. This connects clearly to results obtained from the classical states. That is, in order to measure a quantum system objectively, one has to design a system where the transition between the classical and quantum world is observable.

From this description, open quantum dots offer a unique window on such behavior as they exhibit a mixed classical phase space [18]. Quantum states within these structures that couple well to the outside environment, through the QPC's confining constrictions, are heavily decohered. These states give rise to the chaotic sea [19] that exists in the classical phase space of the dot. Other states within the cavity remain robust throughout this decoherence process, since they do not couple to the leads, and are the pointer states [14,20].This provides a natural connection between the quantum and the classical system, and allows one to study the transition from one to the other [21, 22].

The pointer states represent a subset of the total set of states in the coupled dot plus environment system. This subset can be projected out of the overall system, and represents a set of isolated non-interacting states with its own (projected) Hamiltonian. The real part of this term can lead to the existence of new states [23], but there is also a term that can bring decoherence into the world of the pointer states via electron–electron interactions in the environmental states, a point we have reviewed previously [24]. That is, it represents primarily the environment interaction on the non-pointer states, which can then weakly couple to the pointer states. This term must represent the phase space tunneling by which the pointer states appear in experiment [19]. But, as it also represents the eventual decay of these states through phase-breaking processes, this term must be a non-Hermitian term in the Hamiltonian. In this review, it is this non-Hermitian process which we will discuss and its impact upon the nature of the quantum dots themselves.

2 Experiments in the dots

In the early studies of open quantum dots, there was considerable effort expended to try to establish that the basic behavior of these ballistic quantum dots was governed by *universal* properties that were *generic* in nature and independent of the specific properties of the individual dots. In fact, averaging over e.g. the gate voltage was used to remove the quasi-periodic fluctuations in order to reveal what was believed to be a chaotic background. In fact, this process removed the significant signatures of what we now believe to be the most important aspect of the dots – the pointer states by which the quantum behavior can transition into the classical behavior [14]. In principle, the underlying physics of the ballistic quantum dots is described by characteristics that are dependent upon the individual dot under study, although *there is a*

universal behavior that is characteristic of such dots. That is, the underlying properties, and the characteristic transport through the dots, is governed by the pointer states and their connection to the basic *regular* nature of the semi-classical orbits in the dot [25], but the detailed description of the behavior of any single dot depends upon its peculiar size and structure. Nevertheless, it is this regular nature that is observed as the reproducible fluctuations. The transport is dominated, at low temperature, by reproducible fluctuations which are observed as either a magnetic field, or the gate voltage applied to the dots, is varied. That is, the fluctuations are observed as the Fermi energy, set by the environment, is swept through the spectrum of states. These fluctuations exhibit quasi-periodic oscillations, whose nearly single frequency character is easily discernible in the correlation functions and in the Fourier transforms, and which are endemic to the semi-classical regular orbits in the square quantum dots.

A typical dot defined by depletion metal gates is shown in the lower inset to Fig. 1. For this dot, the gate regions are defined by lift-off of metallic Schottky barrier metals. The dots are basically square in

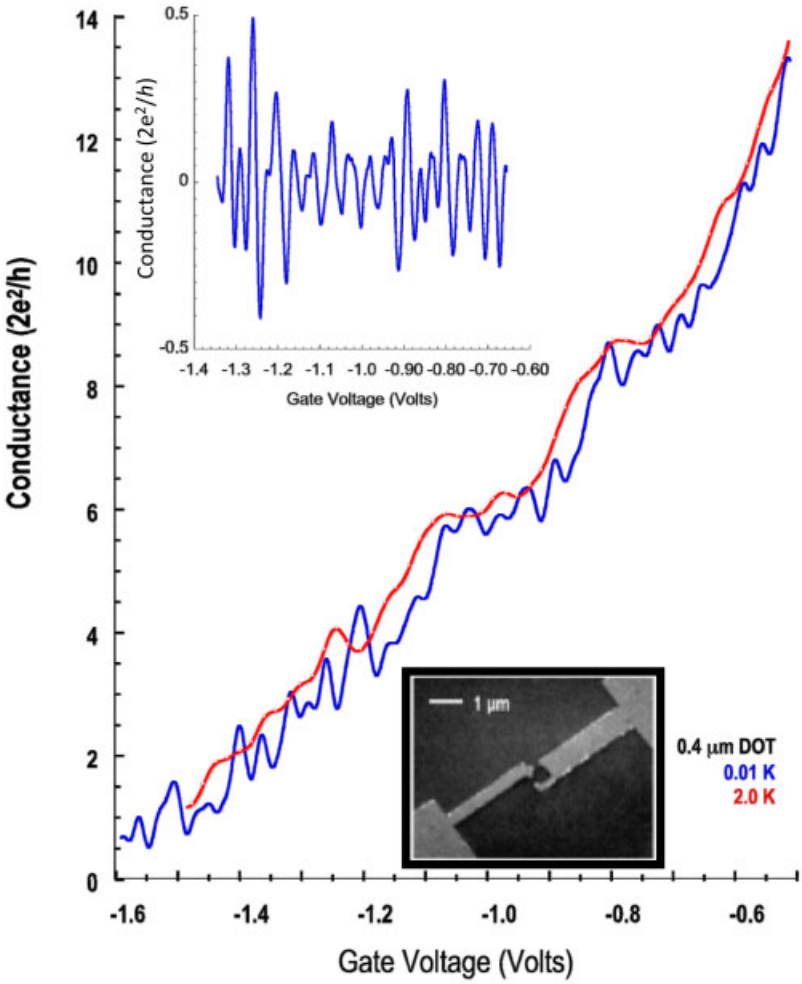

Fig. 1 (online colour at: www.fp-journal.org) The main panel shows the experimental data of conductance as a function of gate voltage at 10 mK (dark, blue curve) and 2 K (light, red curve). The latter is subtracted from the low temperature curve to yield the fluctuations seen in the upper inset. The lower inset is a micrograph of the device.

nature, and sizes ranged from 1.5 μm to 0.4 μm (the electrical sizes are somewhat smaller due to edge depletion around the gates). In nearly all cases studied, the carrier density was 3–5 $\times 10^{11}$ cm^{-2}, and mobilities are typically 40–200 m^2/V-s. The gate design allowed electrons to be trapped in the central square cavity. Measurements were typically carried out at 10–300 mK base temperature in either a dilution refrigerator or a He_3 cryostat, and source-drain excitation was kept well below the thermal voltage with lock-in techniques utilized. When the gate voltage is varied, the actual frequency depends upon both the dot size and the lever arm from the gate voltage to the actual Fermi level motion within the dot. The oscillations often are observed over the entire range of gate voltage and persist to conductance values of $15\ e^2/h$, which represents a very open dot. Here, we will focus upon a smaller dot, whose gate defined dimension varied from 0.2–0.3 micron, depending upon the value of the applied gate voltage. In the main panel of Fig. 1, we plot the conductance through the quantum dot as the gate voltage is varied. It may be seen that the fluctuations ride on a uniformly increasing (for increasing gate voltage) conductance background. Rather than try to smooth the curve, the temperature is raised above 2 K, a point at which the fluctuations are largely damped out, and the background appears as shown in the figure. This background curve is then subtracted from the low temperature curve to isolate the fluctuations themselves, which are plotted as the upper inset in Fig. 1. These oscillations are very nearly periodic with a dominant period of about 15 V^{-1} [26], although there are a few much weaker frequencies in the Fourier spectrum. The experimental results and quantum simulations yield the same dominant frequency in the dots [26]. Moreover, careful studies of the classical trajectories in such a dot have connected these scars to classical states on a KAM island, and matched the corresponding frequencies. Certainly the change in the size of this island and the change in dot size with gate voltage can be connected via careful determination of the self-consistent potential, and this leads to a strong connection between the observed oscillations and the KAM island states [19, 22].

An extensive set of the conduction resonances/fluctuations has been examined for the projection onto the single eigen-states (in each case), and the nature of the resonance has been shown to exhibit a Fano line shape [27]. Here, it is found that the broadening of each resonance is essentially independent of the lead opening of the QPCs, so that the coupling of these states to the external world is through a process of phase space tunneling [19, 28]. That is, the current is assumed to enter the dot via one of the decohered states, tunnel to/from the pointer state, and then leave the dot via a second decohered state.Now, the pointer states and the chaotic decohered states have different statistics. In particular, the classical regular states, and their quantum pointer state counterparts, have classical Poissonian statistics, while the chaotic states are characterized by one of the Gaussian ensembles (the choice depends upon whether or not time reversal symmetry is broken by a magnetic field). In fact, this difference in statistics has been measured in a quantum simulation of the quantum dot [29]. This further serves as a clear connection between the classical and the quantum behavior that arises in these open quantum dots.

We have previously discussed the phase breaking time measurements that we have carried out on these dots [24], so there here we will summarize the results. Generally, these are characterized by two distinct behaviors. At low temperatures, the phase breaking time is independent of temperature, a result generally in keeping with our understanding of the electron–electron interaction in mesoscopic systems [30]. At high temperatures, however, the phase breaking time decreases as a power of the temperature, with the exponent being related to the dimensionality of the system. If the dot is coupled to a large two-dimensional system, this power law is T^{-1} [31]. However, if the dot is coupled to one dimensional wires at each QPC, the power law appears to behave as $T^{-2/3}$ [32]. These results are also consistent with the understanding of the electron–electron interaction in mesoscopic systems [33]. Thus, this high temperature decay seems to indicate that the phase breaking process for the conductance oscillations, which arise from the pointer states, is characterized by the dimensionality of the environment to which the quantum dot is directly attached. That is, the dominant interaction for the phase breaking process arises from many-body interactions between electrons on the pointer state and electrons in the environment. This is a slow process and phase breaking times of the order of a nanosecond can be observed for these open dots. We will return to this point below.

3 The non-Hermitian Hamiltonian

Decoherence is thought to be an important part of the measurement process, especially in selecting the classical results; that is, in passing from the quantum states to the measured classical states of a system [34]. However, the description (and interpretation) of the decoherence process has varied widely, but key is the interaction of the system upon the environment, as well as the interaction of the environment upon the system. Zurek has proposed that the interaction of the system on the environment leads to a preferred, *discrete* set of quantum states, known as *pointer* states, which remain robust, as their superposition with other states, and among themselves, is reduced by the decoherence process [35]. This decoherence-induced selection of the preferred pointer states was termed *einselection* [34]. While this describes the physics of einselection, the mathematics can be shown by the use of projection operators. We give a brief overview here. We consider a system S, interacting with its environment E, so that the combined system plus environment $(S + E)$ is either closed, or influenced by external driving fields that are assumed known and unaffected by the feedback from this combined $S + E$. The Hilbert spaces of both the environment and the system are assumed to be finite dimensional, although this is not critical. These two spaces form a tensor-product Hilbert space of the system plus environment. The operators in which we are interested arecalled *superoperators*, and exist in an expanded space often called the *Liouville* space. When we open the dots, there will be an interaction between the dot and the environment, so that we can write the total Hamiltonian as

$$H = H_S + H_E + H_{\rm int}, \tag{1}$$

where the three terms represent the system, the environment, and the interaction between these two.

There are two crucial steps in defining a reduced density matrix for just the pointer states. The first is to project out these states via a projection superoperator. The second is to then trace over the environmental states yielding just the reduced set of pointer states. This procedure has been known for a considerable time [36–38]. There are many ways to define, or create, the necessary projection operator, which, as mentioned above, is a commutator-generating superoperator. We want to choose the particular projection operator such that

$$\hat{P}\hat{H}\hat{P} = \hat{H}_p, \tag{2}$$

where the "caret" indicates a superoperator. Now, these projection operators are idempotent ($\hat{P}^2 = \hat{P}$), and consequently have eigenvalues of 0 or 1, and it is a central tenet of quantum mechanics that we can build the system through knowledge of the eigen-functions and their eigen-values. For this subsystem, all the eigenvectors are stationary states in the Heisenberg representation [39]. We have used this in an earlier study of open quantum systems [40]. With this approach, we recognize that the pointer states really are a set of isolated states within the dot, and are not directly coupled. Indeed, this approach has been used to create so-called decoherence-free subspaces in quantum information processing [41–43].

We begin by writing the Liouville equation in terms of the composite density matrix ρ, which is defined on a tensor product Hilbert space of the system density matrix and the environment density matrix, as

$$\rho = \rho_s \otimes \rho_e, \tag{3}$$

for which the Liouville equation can be written as

$$i\hbar\frac{\partial\rho}{\partial t} = \hat{H}\rho. \tag{4}$$

In particular, the Hamiltonian is a commutator-generating superoperator. Equation (4) is easier to understand when we see that the Hamiltonian is now a 4th rank tensor, which generates the commutator relation

normally seen in this equation via

$$(\hat{H}\rho)_{kn} = \sum_{rs} \hat{H}_{kn,rs}\rho_{rs} = \sum_{rs} (H_{kr}\rho_{rn} - \rho_{ks}H_{sn}). \tag{5}$$

If the dimension of ρ_s is d_s and the dimension of ρ_e is d_e, then the dimension of the superoperator is $d_s^2 d_e^2$ [40]. To simplify the approach, we Laplace transform (4), and then trace over the environment variables to give [44]

$$\left(i\hbar s - \hat{H}_S\right)\rho_s = Tr(H_{\rm int}\rho) + \rho_s(0), \tag{6}$$

As discussed above, we now use a projection operator which yields the pointer states as eigenfunctions. This operator has the basic properties

$$\rho_{ps} = \hat{P}\rho_s, \quad \hat{P}^2 = \hat{P}, \quad \hat{Q} = \hat{1} - \hat{P}. \tag{7}$$

To proceed, we need only to use an identity that is obtained by projecting the Liouville equation with both $\hat{P}$ and $\hat{Q}$, solving for $\hat{Q}\rho_s$ to formally decouple these two equations and recombining the terms [40, 45]. This identity is

$$\frac{1}{i\hbar s - \hat{H}} = \left(\hat{P} + \hat{Q}\hat{R}\hat{Q}\hat{H}\hat{P}\right)\frac{1}{i\hbar s - \hat{C} - \hat{P}\hat{H}\hat{P}}\left(\hat{P} + \hat{P}\hat{H}\hat{Q}\hat{R}\right) + \hat{P}\hat{H}\hat{Q}\hat{R}\hat{Q}\hat{H}\hat{P} \tag{8}$$

where

$$\hat{R} = \frac{1}{i\hbar s - \hat{Q}\hat{H}\hat{Q}}, \qquad \hat{C} = \hat{P}\hat{H}\hat{Q}\hat{R}\hat{Q}\hat{H}\hat{P}. \tag{9}$$

The last term is a "collision" type term which connects the environment to the device via the off-diagonal elements of the superoperator. If we now define some further reduced parameters as

$$\hat{\Sigma}\rho_{ps} = Tr_e\left(\hat{C}\rho_{ps}\right), \qquad \hat{H}'_{\rm int}\rho_{ps} = Tr_e\left(\hat{P}\hat{H}_{\rm int}\hat{P}\rho_s\right) \tag{10}$$

we can then write the reduced equation as

$$i\hbar\left(s\rho_{ps} - \rho_{ps}(0)\right) = \hat{H}_{ps}\rho_{ps} + \hat{\Sigma}\rho_{ps} + \hat{H}'_{\rm int}\rho_{ps} + i\hbar Tr_e\left(\hat{P}\hat{H}\hat{Q}\hat{R}\hat{Q}\rho_s(0)\right) \tag{11}$$

In general, we are seeking the steady-state, long-time limit, and would ignore the initial conditions. However, the last term in (11) has been suggested as contributing to the random force [46] that appears in e.g. the Langevin equation as well as to screening [47], so that it may not be proper to totally ignore it. However, the final long-time limit equation becomes, after inverting the Laplace transform,

$$i\hbar\frac{\partial\rho_{ps}}{\partial t} = \left(\hat{H}_{ps} + \hat{H}'_{\rm int}\right)\rho_{ps} + \hat{\Sigma}\rho_{ps} \tag{12}$$

The second term on the right hand side is not a scattering, or decoherence term, as that would appear in the last term on the right. Instead, it represents a weak interaction between the pointer states and the environment *via the decohered states*. That is, it represents primarily the environment interaction on the non-pointer states, which can then weakly couple to the pointer states. This term must represent the phase space tunneling by which the pointer states appear in experiment [19]. It is true, however, that this can bring decoherence into the world of the pointer states via electron–electron interactions in the environmental states, a point we have reviewed previously [24]. Normally, the pointer states do not interact with the environment, so that the last term would vanish, but the interaction of the pointer states, through the decohered states, to the environment produces the phase breaking discussed in the previous section. This means that the last term *does not vanish*, but represents this phase breaking process through an imaginary term in this self-description. Since this scattering term is part of the Hamiltonian of the pointer states (the reduced set of states), it is a diagonal term, but has an imaginary part, which makes the Hamiltonian non-Hermitian.

It is important to remark here that this form of Hamiltonian is not what one normally refers to as non-Hermitian. Here, the imaginary term which breaks up the Hermitian properties lies on the diagonal of the matrix. In essence, this will also make the resulting reduced density matrix non-norm conserving as it breaks up the unity of the trace. But, this is because the germane interactions are from states within the dot and states of the environment, which can include renormalized decohered states of the dot. This environment sensitive dephasing interaction is seen in experiment [24], as discussed above. The steady-state situation has to then account for lost amplitude in the dot being replaced by electrons injected from the environment itself. These source terms must be incorporated within the first term on the right-hand side of (12) as in any other transport problem.

Now, there are further problems with (12). While it appears to be quite simple conceptually, this is not really the case. First, within the partial trace in both terms of (10), there is an explicit dependence on the choice of the projection operator $\hat{P}$ or, equivalently, on the environment density matrix that induces the projection operator, so one must make a choice of the latter to actually be able to use (12). At the end of the day, the equation of motion for $\rho_S(t)$ should not depend on it. And yet it does through its affects on the projection operator. The rationale for believing that the equation of motion for $\rho_S(t)$ should not depend on the details of the environment goes back to our statement above that the eigen-states of $\rho_S(t)$ are our pointer states, and these are properties of the specific dot, and exist in the dot for a variety of different environments. We have previously shown [40] that quite generally, the eigen-space of the projection operator, corresponding to those states with eigenvalue 1, must be isomorphic to the states of $\rho_S(t)$, which are our pointer states.

4 Quantum simulations

Since the pointer states conpose a reduced system, one must identify them before a projection operator can be put together (which is mostly after we have the desired information). In general, this means a simulation of the quantum transport through the open quantum dot(s). Our method of choice for carrying out the quantum transport studies is one originally developed by Usuki and coworkers [48, 49]. It is a technique closely related to the cascading scattering matrix approach, as well as the Green's function approach which may be the most popular method for carrying out these kinds ofcalculations. The Usuki technique however has a major advantage over the latter, as we will describe.

The starting point for our approach is a general Hamiltonian which is discretized upon a rectilinear grid [50]. While it is easy to incorporate the magnetic field, this approach has been extended to treat dissipation in nanowire transistors [51] and to incorporate spin and the Rashba and Dresselhaus spin-orbit terms [52]. On the grid, a tridiagonal matrix represents the Hamiltonian for the individual isolated slices I, where a slice is the column of the grid normal to the direction of current flow. Expanding the Schrödinger equation discretization, one obtains an iterative equation for one slice in terms of the previous ones, which is a form of the Lippmann-Schwinger equation on the grid. Coupling this with the trivial equation that the

slice wave function vectors are equal to each other, one can derive a transfer-matrix equation that relates adjacent slices, as

$$\begin{bmatrix} \vec{\psi}_i \\ \vec{\psi}_{i+1} \end{bmatrix} = \begin{bmatrix} 0 & \mathbf{I} \\ -\mathbf{I} & \left(\dfrac{\mathbf{H_{0i}} - E}{t}\right) \end{bmatrix} \begin{bmatrix} \vec{\psi}_{i-1} \\ \vec{\psi}_i \end{bmatrix} = \mathbf{T_i} \begin{bmatrix} \vec{\psi}_{i-1} \\ \vec{\psi}_i \end{bmatrix} \tag{13}$$

where $t = \hbar^2/(2m^*a^2)$ is the hopping matrix element from one site to the next. Here, this acts as a weak perturbation coupling one slice to the next, and is of course modified in a magnetic field via the Peierls' phase. One begins the calculation by turning to Bloch's theorem, and solving the eigenvalue problem for the transfer-matrix on the first slice (the T matrix carries throughout by coupling one slice to the next)

$$\mathbf{T}_1 \begin{bmatrix} \vec{\psi}_1 \\ \vec{\psi}_0 \end{bmatrix} = \begin{bmatrix} \mathbf{T}_{11} & \mathbf{T}_{12} \\ \mathbf{T}_{12} & \mathbf{T}_{22} \end{bmatrix} \begin{bmatrix} \vec{\psi}_1 \\ \vec{\psi}_0 \end{bmatrix} = \lambda \begin{bmatrix} \vec{\psi}_1 \\ \vec{\psi}_0 \end{bmatrix}. \tag{14}$$

Once one has passed the initialization of the transfer matrices with the initial conditions on the wave function, which are defined through the matrices $\mathbf{C}_1^0 = \mathbf{I}$ and $\mathbf{C}_2^0 = \mathbf{0}$. These are defined for the zero slice. Then the general iteration becomes

$$\begin{bmatrix} \mathbf{C}_1^{l+1} & \mathbf{C}_2^{l+1} \\ \mathbf{0} & \mathbf{I} \end{bmatrix} = \mathbf{T}_l \begin{bmatrix} \mathbf{C}_1^{l} & \mathbf{C}_2^{l} \\ \mathbf{0} & \mathbf{I} \end{bmatrix} \mathbf{P}_l, \tag{15}$$

where

$$\mathbf{P}_l = \begin{bmatrix} \mathbf{I} & \mathbf{0} \\ \mathbf{P}_{l1} & \mathbf{P}_{l1} \end{bmatrix}, \tag{16a}$$

with

$$\mathbf{P}_{l1} = -\mathbf{P}_{l2}\mathbf{T}_{l21}\mathbf{C}_1^l, \tag{16b}$$

and

$$\mathbf{P}_{l2} = \left(\mathbf{T}_{l21}\mathbf{C}_2^l + \mathbf{T}_{l22}\right)^{-1}. \tag{16c}$$

The numerical stability of the Usuki et al. method in large part stems from the fact that the iteration implied by (15) involves products of matrices with *inverted* matrices. Taking such products tends to cancel out most of the troublesome exponential factors.

In Fig. 2, we display a scarred wave function which is found in a nominally 0.3 μm square dot with 40 nm QPCs, located at the top edge of the dot (it is possible to note the modes which are passing through these QPCs at the top of the figure), which pass three modes. This wave function appears periodically in magnetic field, almost always with essentially the same shape, and thus is one of the pointer states. This state is very long lived and clearly identified with the dot itself. Moreover, it is found that this scarred state scales with the dot size [53,54]. The wave function shown in Fig. 2 is clearly scarred by a periodic classical orbit. However, since the structure is ostensibly regular, the fact that there appears to be a correspondence to the classical picture should not be a surprise (as pointed out above) since the wave functions should be concentrated along the projections of the invariant tori of the regular trajectories in classical phase space. However, it is worth pointing out that this image *differs radically* from what occurs in a *closed* dot, in which the amplitude for an eigenstate is distributed much more uniformly and one *can not* make an association with a single orbit. It is also worth noting that this wave function does not have significant amplitude at the QPCs, but is basically isolated from them.

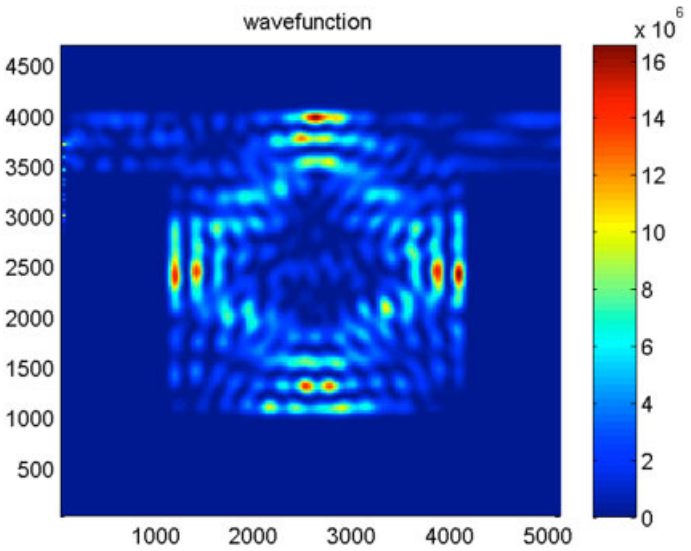

Fig. 2 (online colour at: www.fp-journal.org) A pointer state that is found within a quantum dot by simulation of the quantum transport through the dot.

5 Trapping the pointer states

As discussed above, the pointer states could be investigated using external measurements, and in the past this was about the only way in which to infer their presence. However, the recent advent of scanning gate microscopy (SGM) [55] has allowed the probing of quantum structures within constrictions by rastering a biased AFM tip over the area of interest while concurrently mapping the resulting variations in conductance. This technique has been applied to investigate the quantum Hall edge states and localized regions of quantum point contacts (QPC) [56–58] as well as the classical and quantum behaviors within quantum dots in a GaAs/AlGaAs heterojunction material [59, 60]. In this section, we review what we believe to be the definitive measurement of pointer state scars in a quantum dot in InAs. The use of InAs follows from its higher g-factor, and therefore more pronounced response to a magnetic field. We discuss primarily the images of the scarring state shown in Fig. 2, which is periodic in magnetic field as expected from earlier considerations.

The heterostructure material used in this study consists of first a 1.5 μm strain-relaxed $Al_{0.7}Ga_{0.3}Sb$ layer, which is followed by a 12 nm InAs quantum well (this is the transport layer).Then, a thin $In_{0.2}Al_{0.8}Sb$ confinement layer in which Tellurium is used as a delta dopant, is grown, and finally a 2 nm InAs cap layer (etched off in processing). The latter improves the ability of making ohmic contacts to the sample. The quantum dot geometry was defined using electron beam lithography and then etched into the sample to constrict transport through in-plane quantum point contacts (QPC), as shown in the inset to Fig. 3, which is an AFM image of the active sample area. This technique is preferable to top metal gates in SGM measurements, as it avoids interference between surface metal gates and the scanning gate tip [60, 61]. The dot was designed with inner dimensions of 1.1×1.1 μm and the QPCs on either side have 450 nm openings and 100 nm length, although all of these dimensions are reduced by surface depletion on the sides of the structure. After bonding to the contacts is complete, a thin layer of polymethyl methacrylate is spun onto the sample and baked, in order to insulate the sample from the SGM tip. This process results in a total distance from the PMMA surface to the InAs transport layer of 40 nm. The sample is mounted to the stage of an Omicron low temperature AFM head, which in turn is mounted in a ^{3}He cryostat. Measurements proceed using usual lock-in amplifier techniques under constant current conditions, at a

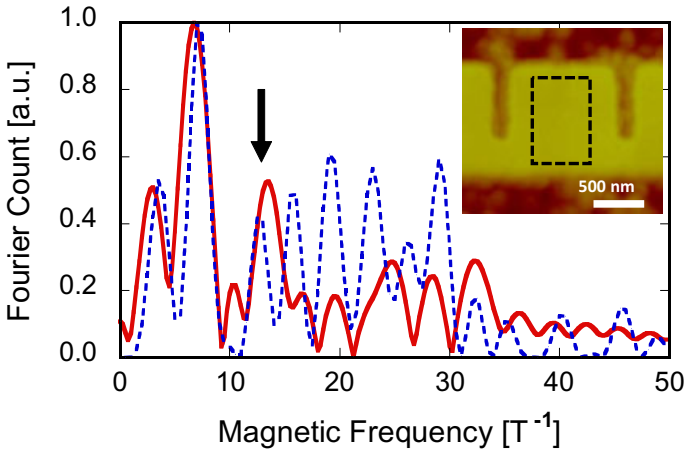

Fig. 3 (online colour at: www.fp-journal.org) The Fourier transform spectrum of the experimental (solid) and simulated (dashed) magnetoconductance. The arrow indicates a Fourier peak of particular interest. The inset is an AFM image of the sample and the dashed box indicates the scan area.

sample temperature of 280 mK. The cryostat system is isolated on three Minus-K vibration isolation tables, and a super-conducting magnet in the dewar provides a magnetic field perpendicular to the electron flow within the sample. Shubnikov-de Haas measurements yield a 2DEG density of 1.5×10^{12} cm^{-2} and a mobility of 65 000 cm^2/Vs.The SGM tip is a piezoresistive AFM tip, which is metalized using 15 nm Cr, to allow the negative DC bias to be applied to create the necessary perturbation. The SGM technique employs this biased tip, at a constant lift height above the sample surface, to raster over an area of interest and act as a local perturbation. The scan area is indicated by the dashed box overlaid on the sample image in Fig. 3.

The magnetoconductance fluctuations in are found by removing the underlying background, as was done for Fig. 1. A Fourier transform in magnetic field is then taken to obtain the resulting frequency spectrum of the correlation function of the fluctuations. The Fourier spectrum is plotted in Fig. 3. The experimental Fourier transform (the solid line) shows peaks at 3.0 T^{-1}, 6.7 T^{-1} and 13.5 T^{-1}. Superimposed on the experimental Fourier transform is the transform of the fluctuations obtained from a simulation (the dashed line), as discussed in the previous section. As noted above, simulations are done at 0 K, so the theoretical trace was smoothed before doing the analysis. Note that the three lowest peaks of the Fourier transform line up closely, with the highest of the three being slightly lower than the experiment, 12.7 T^{-1}.With the preceding discussion of periodic scarring effects in mind, a series of SGM images was taken every 10 mT ranging from 0 to 350 mT. Each image consists of 120 raster scans across the image area, designated by the dashed line in the inset to Fig. 3 [62].

In Fig. 4, we plot the individual images from the SGM scans. Here, the image at 0 mT has been subtracted from each other image in order to emphasize the magnetic field dependent features. Nevertheless, the features within the scan are masked by the background. To remove the background, and to highlight the periodic features that occur in the scans, we compute the Fourier transform, with respect to magnetic field, over the entire set of images. Because the device magnetoconductance is symmetric in B, a cosine transform was used. This incorporates a phase shift appropriate to magnetic fields which exhibited peaks in analysis of the magnetic progression of scan rows (not shown). The equation for the transform becomes:

$$F(\omega) = \int I(B)\cos(\omega B + \varphi)dB \tag{17}$$

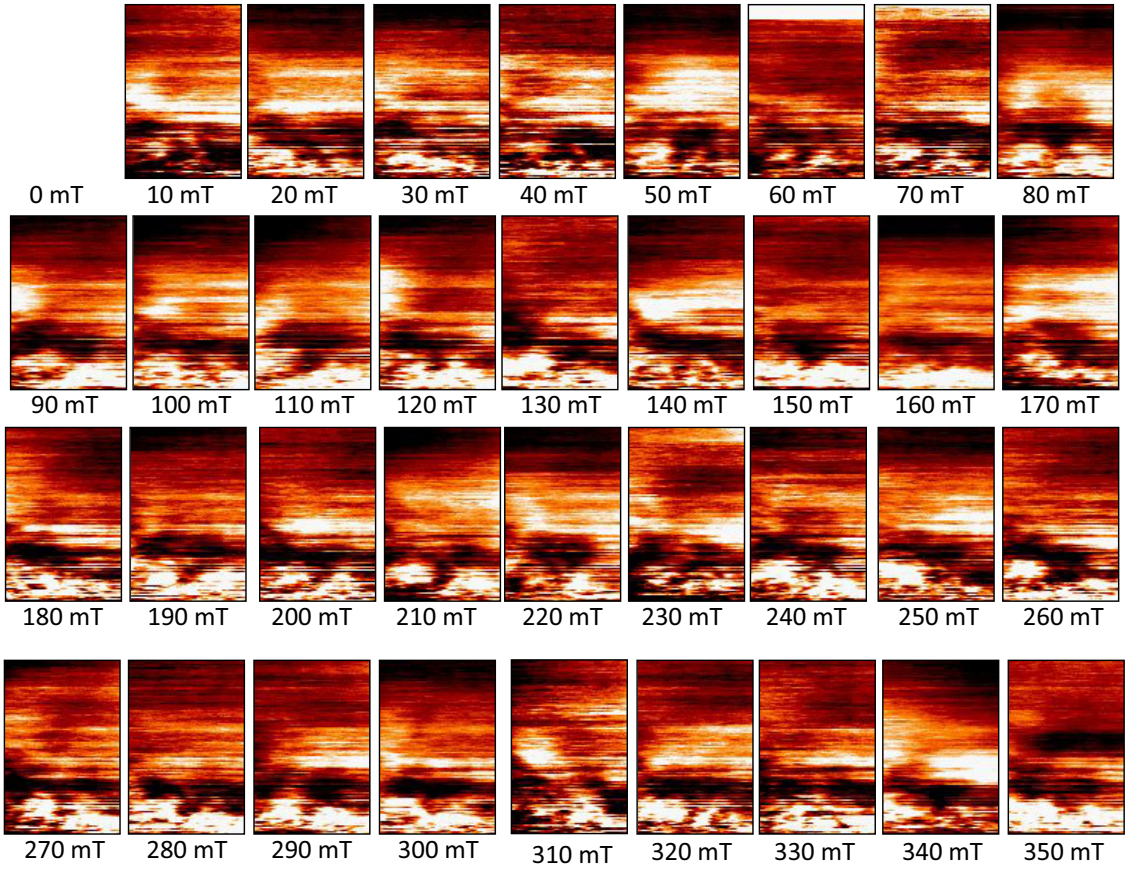

Fig. 4 (online colour at: www.fp-journal.org) Images of the SGM scans of the sample. Here, the scan area is 576×876 nm^2. The image at 0 mT has been subtracted from each other image to emphasize the magnetic field dependence.

where $I(B)$ is the image at each magnetic field, ω is the frequency $(2\pi f)$, f is the magnetic frequency, and φ is the shift in phase to align the function to a known peak in B. The relative phase shift was adjusted to find the best response, and the transform was run over a wide range of magnetic frequencies. From this, it was found that there were two resulting magnetic frequencies that gave higher overall meaningful pictures of the periodic scar structures. These images occurred at frequencies of 7 and 13.5 T^{-1}, which exhibits excellent agreement with the peaks shown in Fig. 3. It is the 13.5 T^{-1} magnetic frequency result that is of most interest to us, however. This latter state produced is shown in Fig. 5(a) [62]. This state strongly resembles the "diamond" scar shown in Fig. 2. The simulation of the present device also yields the "diamond" state, although it is not as distinct due to the much larger size of the dot used in the experiments. Note that the field spacing coincides with the Fourier peak of 12.7 T^{-1} obtained from the analysis of the theoretical conductance trace.

The diamond scar shown in Fig. 2 corresponds to a pristine sample. In fact, the pointer states exist because they do not connect to the environmental states. On the other hand, SGM corresponds to an intrusive procedure in which the environment is brought into the quantum dot. To account for this, the simulation procedure was changed to account for the scanning gate perturbation, with a consequent measurement of the conductance. This perturbation has significant effect upon the scarred state. In Fig. 5(b), we show a simulation of the SGM measurement with the conditions (Fermi energy, magnetic field, etc.) corresponding to the presence of the diamond scar. While not perfect, there is a significant correlation between the

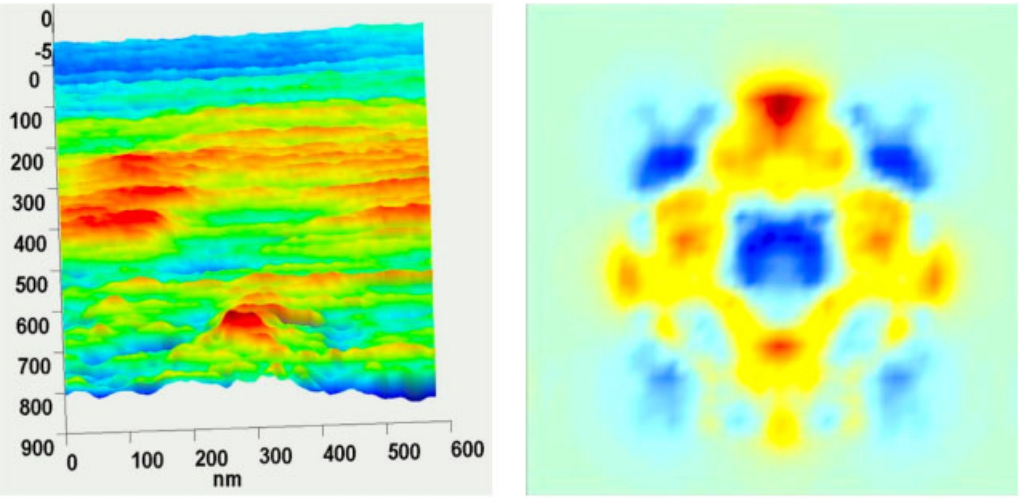

Fig. 5 (online colour at: www.fp-journal.org) (a) The Fourier transformed (in magnetic field) image showing remnants of the diamond scarred state. (b) The simulation of the diamond scar subjected to the perturbation of a rastered bias probe, corresponding to the SGM measurements. The agreement is fairly good.

two images. We interpret this agreement as strong evidence for the existence of the pointer states and their importance for the decoherence theory of quantum mechanics.

6 Conclusions

In this review, we have discussed a physical system in which the quantum dynamics is governed by a non-Hermitian Hamiltonian. Here, the non-hermiticity arises primarily because the residual quantum states of the open system comprise a set of pointer states which primarily do not interact with the environmental states. Rather, these states would be considered as a decoherence free subspace of the overall system. However, current carrying states, arising from the decohered states which couple intrinsically to the environmental states, can weakly couple to the pointer states via phase-space tunneling. This allows the electrons of the pointer states to interact very weakly with the environmental electrons via a long-range coulomb interaction, and this process leads to the overall phase breaking of the system [24].

The presence of the pointer states is exhibited by conductance fluctuations that arise as the Fermi energy is swept past their energy level when a gate voltage or a magnetic field is swept. These conductance fluctuations are characterized by Fano lineshapes as expected for tunnel coupling. The presence of the electron density on the wave function of the pointer states also has been probed via SGM techniques. Here, the conductance through the quantum dot exhibits changes as the biased AFM tip is swept over the peak of the wave function amplitude. Quite similar shapes for the SGM signal are found from simulations of the quantum transport through the dot with a probing potential present. The conclusion is that the pointer states are real and can be imaged with SGM even thought they do not like to interact with the environment (also represented by the SGM tip). The fact that the fundamental scarred state is found in the dot, regardless of the electron density, is a facet of quantum Darwinism [16, 62], which reinforces the idea of the stability of these states.

References

[1] J. A. Wheeler and W. H. Zurek, (eds.) Quantum Theory and Measurement (Princeton University Press, Princeton, NJ, 1983).
[2] J. P. Bird, R. Akis, D. K. Ferry, and M. Stopa, in: Advances in Imaging and Electron Physics, Vol. 107, edited by P. Hawkes (Academic Press, San Diego, 1999, pp. 1–71.
[3] C. W. J. Beenakker and H. van Houten, Solid State Phys. **44**, 1 (1991).
[4] C. M. Marcus et al., Phys. Rev. Lett. **69**, 506 (1992).
[5] A. M. Chang et al., Phys. Rev. Lett. **73**, 2111 (1994).
[6] R. P. Taylor et al., Phys. Rev. B **51**, 9801 (1995).
[7] J. P. Bird et al., Phys. Rev. B **51**, 18037 (1995).
[8] M. Persson et al., Phys. Rev. B **52**, 8921 (1995).
[9] M. W. Keller et al., Phys. Rev B **53**, R1693 (1996).
[10] R. A. Jalabert, H. U. Baranger, and A. D. Stone, Phys. Rev. Lett. **65**, 2442 (1990).
[11] H. U. Baranger, R. A. Jalabert, and A. D. Stone, Phys. Rev. Lett. **70**, 3876 (1993).
[12] R. Akis, D. K. Ferry, and J. P. Bird, Phys. Rev. B **54**, 17705 (1996).
[13] R. Akis, D. K. Ferry, and J. P. Bird, Phys. Rev. Lett. **79**, 123 (1997).
[14] W. H. Zurek, Rev. Mod. Phys. **75**, 715 (2003).
[15] H. Ollivier, D. Poulin, and W. H. Zurek, Phys. Rev. Lett. **93**, 220401 (2004).
[16] R. Blume-Kohout and W. H. Zurek, Phys. Rev. Lett. **101**, 240405 (2008).
[17] C. Darwin, The Origin of Species (Jon Murray, London, 1859).
[18] R. Ketzmerick, Phys. Rev. B **54**, 10841 (1996).
[19] A. P. S. De Moura et al., Phys. Rev. Lett. **88**, 236804 (2002).
[20] D. K. Ferry, R. Akis, and J. P. Bird, Phys. Rev. Lett. **93**, 026803 (2004).
[21] D. K. Ferry et al., Semicond. Sci. Technol. **26**, 043001 (2011).
[22] R. Brunner et al., J. Phys., Condens. Matter. (in press).
[23] R. Brunner et al., Phys. Rev. Lett. **101**, 024102 (2008).
[24] D. K. Ferry, R. Akis, and J. P. Bird, J. Phys., Condens. Matter. **17**, 1017 (2005).
[25] J. P. Bird et al., Rep. Progr. Phys. **66**, 583 (2003).
[26] J. P. Bird et al., Phys. Rev. Lett. **82**, 4691 (1999).
[27] R. Akis, J. P. Bird, and D. K. Ferry, Microelectron. Eng. **63**, 241 (2002).
[28] R. Akis et al., J. Comput. Electron. **2**, 281 (2003).
[29] R. Akis and D. K. Ferry, Physica E **34**, 460 (2006).
[30] D. K. Ferry, Semiconductor Transport (Taylor & Francis, London, 2000) pp. 355–359.
[31] J. P. Bird et al., Phys. Status Solidi (b) **204**, 314 (1997).
[32] D. P. Pivin Jr. et al., Phys. Rev. Lett. **82**, 4687 (1999).
[33] B. L. Altshuler, A. G. Aronov, and D. E. Khmelnitsky, J. Phys. C **15**, 7367 (1982).
[34] W. H. Zurek, Phys. Rev. D **26**, 1862 (1982).
[35] W. H. Zurek, Phys. Rev. D **24**, 1516 (1981).
[36] S. Nakajima, Prog. Theor. Phys. **20**, 948 (1958).
[37] R. Zwanzig, J. Chem. Phys. **33**, 1338 (1960).
[38] H. Mori, Prog. Theor. Phys. **33**, 423 (1965).
[39] P. A. M. Dirac, The Principles of Quantum Mechanics, 4th edition (Oxford University Press, London, 1958).
[40] I. Knezevic and D. K. Ferry, Phys. Rev. E **66**, 016131 (2002).
[41] L. M. Duan and G. C. Guo, Phys. Rev. A **57**, 737 (1998).
[42] P. Zanardi and M. Rasetti, Phys. Rev. Lett. **79**, 3306 (1997).
[43] D. A. Lidar, I. L. Chuang, and K. B. Whaley, Phys. Rev. Lett. **81**, 2594 (1998).
[44] D. K. Ferry, Semiconductors, Chapter 15 (Macmillan, New York, 1991).
[45] J. R. Barker, Solid-State Electron. **21**, 197 (1978).
[46] N. Pottier, Physica A **117**, 243 (1983).
[47] J. R. Barker, in: Physics of Nonlinear Transport in Semiconductors, edited by D. K. Ferry, J. R. Barker, and C. Jacoboni (Plenum Press, New York, 1979).
[48] T. Usuki et al., Phys. Rev. B **50**, 7615 (1994).

[49] T. Usuki et al., Phys. Rev. B **52**, 8244 (1995).
[50] R. Akis et al., in: Electron Transport in Quantum Dots, edited by J. P. Bird (Kluwer Academic Publishers, Boston, 2003) pp. 209–276.
[51] M. J. Gilbert, R. Akis, and D. K. Ferry, J. Appl. Phys. **98**, 094303 (2005).
[52] A. W. Cummings, R. Akis, and D. K. Ferry, J. Phys., Condens. Matter. **23**, 465301 (2011).
[53] J. P. Bird et al., Chaos, Solitons, Fractals **8**, 1299 (1997).
[54] D. K. Ferry et al., Jpn. J. Appl. Phys. **36**, 3944 (1997).
[55] M. A. Topinka et al., Science **289**, 2323 (2000).
[56] R. Crook et al., J. Phys. Cond. Matt. **12**, L167 (2000).
[57] N. Aoki et al., Phys. Rev. B **72**, 155327 (2005).
[58] C. R. da Cunha et al., Appl. Phys. Lett. **89**, 242109 (2006).
[59] R. Crook et al., Phys. Rev. Lett. **91** 246803 (2003).
[60] A. M. Burke et al., J. Vac. Sci. Technol. B **26**, 1488 (2008).
[61] A. M. Burke et al., J. Phys., Condens. Matter. **21**, 202201 (2009).
[62] A. M. Burke et al., Phys. Rev. Lett. **104**, 176801 (2010).

